INTERNATIONAL JOURNAL FOR NUMERICAL AND ANALYTICAL METHODS IN GEOMECHANICS
*Int. J. Numer. Anal. Meth. Geomech.*, **23,** 647–671 (1999)

# A LATTICE TYPE MODEL FOR PARTICULATE MEDIA

MUNIRAM BUDHU*,†, S. RAMAKRISHNAN‡, AND GEORGE FRANTZISKONIS§

*Dept. Civil Engrg. & Engineering Mechanics, University of Arizona, Tucson, AZ-85721, USA*

## SUMMARY

In this paper, a lattice-type model to simulate the micro-mechanical behaviour of particulate/granular media is presented. In this numerical model, a particulate assembly is simulated as a lattice/truss. Nodes located at contacts between a particle and its neighbours are linked by bars to each other. Each particle is represented by a lattice within its microstructure and particle interact through load transfer at the nodes. Constraints are prescribed at the nodes to describe active, deactivated and reactivated contacts. When a particulate assembly develops into a mechanism (deformation with zero incremental load), further deformation is simulated through a framework that describes the kinematics of the particles (sliding, rolling and rotation of particles). This framework is formed by introducing nodes at the particle centroids and linking them with bars. Bars-linking particles with a non-sliding contact are assigned large stiffnesses relative to bars linking particles with a sliding contact. Numerical tests are conducted on two-dimensional assemblies of disks, arranged as very loose and very dense packing under simple shear loading conditions. The results concord with the results of numerical tests conducted using the discrete element method and with photoelastic experiments. Additionally, the model is applied to study the effects of initial imperfections caused by particles with low elastic modulus. Copyright © 1999 John Wiley & Sons, Ltd.

Key words: mechanics; granular; particulate; materials; lattice; trusses; simulation; modeling

## INTRODUCTION

The mechanical behaviour of particulate/granular materials, composed of mutually contracting particles or structural units, under various loads and environmental conditions has generated considerable interest. Their behaviour is governed by the size, shape, roughness, relative position and strength of the particles, and of the nature of interaction between the particles.[1] The deformation of particulate materials, of which geomaterials are a subset, is predominantly caused by the mutual sliding, rotation and rolling of particles (intergranular deformation), in contrast to "continuums" (e.g. crystalline materials) in which the deformation of the individual grains (intragranular deformation) is predominant. Continuum theories have been applied to understand the mechanical behaviour of particulate materials, the main drawback being that they do not account for the micro structural effects.

Several analytical and numerical techniques have been developed to understand the particulate material behaviour since the availability of Hertz's solution[2] for two deformable elastic bodies in

*Correspondence to: Dept. Civil Engrg. & Engineering Mechanics, University of Arizona, Tucson, AZ-85721, USA
†Professor
‡Grad. Student
§Associate Professor

CCC 0363–9061/99/070647–25$17.50

*Received 23 July 1997*
*Revised 22 May 1998*

contact. Serrano and Rodriguez-Ortiz[3] developed a numerical model for disk/sphere assemblies in which the disks were assumed to be rigid and were linked at contacts by normal and tangential springs. The normal and tangential stiffness were derived from the contact theories of Hertz[2] and Mindlin.[4] A modification of this model by Cundall and Strack[5] led to the development of a powerful numerical technique called the Discrete Element Method (DEM). This method has been successfully applied to the study of the mechanical behaviour of particulate/granular assemblies. Since the development of DEM, several aspects of particulate material behaviour have been investigated and these can be found in the works of.[6–9] Using the particle assembly composed of rigid disks with interactions through Hertz-Mindilin contact stiffnesses, either as improvements to DEM or as alternative approaches to DEM, several numerical methods and theories have been developed to describe particulate material behaviour.[10–13]

An alternative method and one that has a growing interest among physicists and engineers is the study of the behaviour of materials through network models.[1,14–20] Hermann and Roux[16] showed that network models are particularly good for analyses of dilution processes (sequential removal of links in the lattice) and the determination of the influence of disorder introduced by a random spatial distribution of the link parameters. Two important features of network models or lattice-type models are (a) the ability to consider complex states of stress and strain and (b) efficiency in providing estimates of the influence of stress concentrations and spatial correlations of defects on the macro-response of the system.

The interests of engineers have been either to develop continuum-like models for materials with lattice-like microstructure or to use lattices for the analysis of continuum. The relationship between a continuum and a network/lattice was first examined in some early works by Hrennikoff[21] and later by Newmark.[22] These works involved analysing a continuum by replacing it with an equivalent elastic network. The reverse possibility of replacing a large repetitive network with an equivalent continuum was studied by Kollar and Hegedus (1985),[23] Dow *et al.*[24] and Noor and Russell.[25] These studies presented methods to simplify certain calculations for large space trusses and space frames. Lattice models applied to particulate media[19,20] were intended to capture the discrete load paths that are inherent in the transmission of loads within the materials. These models were limited in their application to granular assemblies with indestructible contacts and thus the changes in fabric due to activated and deactivated contracts were not included.

In this paper, a lattice type model (LTM) that is distinctly different from the network approaches of Trollope and Burman[20] and Sadd *et al.*[19] is presented. In contrast to the above approaches, where the lattice was formed by linking particle centroids, we replace each particle by a network of bars and each network is linked to its neighbor by nodes at the particle contacts. The major objective of this paper is to present the concepts in formulating the lattice type model and the results from numerical tests conducted on idealized particulate media.

## MODEL FORMULATION

### *General concepts*

In the lattice-type simulation of a two-dimensional assembly of particles, the assembly is modelled as a network of bars linking nodes introduced at particle contacts (Figure 1). A contact node on a particle is linked to every other node on that particle. Each particle is treated as an independent entity (material properties and geometry) that interacts with its neighbours at

 

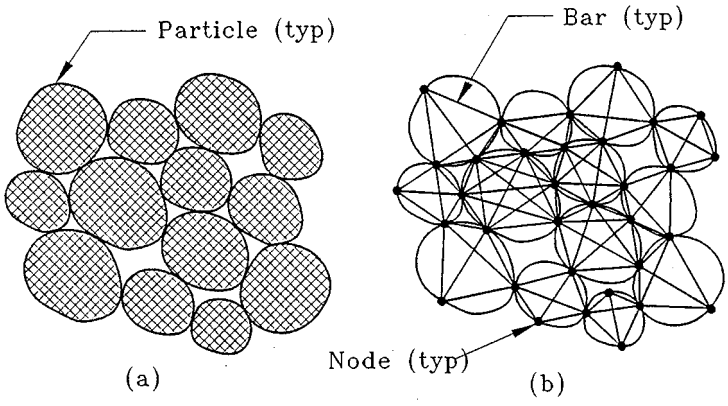


Figure 1. (a) Particle arrangement; (b) Lattice type simulation

contact nodes. If the number of contacts around a particle is less than four, then inactive nodes are introduced around the particle to obtain a minimum of four nodes. This is needed because, during the deformation process, the trajectory of the centroid of a particle is traced from the displacement of the centroid of the polygon formed by linking the contacts and thus it is reasonable to link contacts rather than particle centroids. We began the work by simulating the lattice by introducing nodes both at particle contacts and particle centroids and linking the nodes with bars.[26,27] Even though the results were in general agreement with the behaviour of particulate media, it was found that the method can lead to erroneous results. The results and the limitations of this approach are extensively discussed by Ramakrishnan.[26]

For two-dimensional particle systems, the network becomes a statically indeterminate two-dimensional truss while for a three-dimensional array of particles, a space truss is obtained. Constraints are imposed at the nodes to describe activated, deactivated and reactivated contacts. Standard matrix method of structural analysis is then used to determine the displacements at nodal points and the axial forces in the bars due to imposed loads or displacements at the boundary nodes. Two key parts of the modelling approach are the numerical implementation of the constraint conditions and the kinematics to mimic the material responses. We describe, in this paper, the methodology we developed and the input data required to handle the constraint conditions and the kinematics.

*Data requirements*

The input data required for a truss analysis are the geometric properties—lengths and areas—of the bars and the material property—elastic modulus. The lengths of the bars ($L$) depend on the geometry of the particles and the location of the contact points. Particles of irregular shape can be approximated as disks of circular/elliptical cross sections or mapped using the theory of morphology.[28] However, in this paper we will only discuss particles of circular cross sections but the analysis with some modifications can be applied to disks of different shapes.

The areas of the bars ($A$) are unknown as they depend on the contact forces and the elastic modulus of each particle. The challenge is to determine how the bar areas should be determined

 

and we describe below how this is done. The elastic modulus of the bars ($E$) within a particle is assumed to be equal to the elastic modulus of the particle which can be determined for single grains in a similar way to Mindlin.[4] Each particle or bars within a particle can have different elastic modulus to characterize initial anisotropy or initial imperfections in a particulate medium. With these parameters (lengths, areas and elastic moduli), the truss is analysed for a given load under appropriate boundary conditions and the nodal displacements and axial forces in the bars are determined.

*Bar Areas*

In the LTM, the initial areas of the bars have to be assigned and adjustments have to be made after each loading increments based on the axial forces in the bars. The latter is analogous to the changes in contact area between two elastic deformable impinging disks resulting from changes in loadings. The areas of the bars within a particle are found by assuming that the particle is an elastic disk. The displacements at the nodal points of the disk under the resultant forces at the nodes are computed from theory of elasticity and the area of each bar is determined according to the displacement in the direction of the bar as described below.

The displacements of the contact nodes in a disk acted upon by a set of contact forces (Figure 2) are computed from the solution for stresses derived by Michell[29] (see Appendix I) as applied by Timoshenko and Goodier[30] for a disk problem. The displacements of the contacts are resolved in the direction of each bar and the bar areas are then updated using

$$A_j = \frac{F_j L_j}{E_j \delta_j} \tag{1}$$

where $A_j$ is the cross-sectional area of bar '$j$'; $F_j$ the axial force in the bar; $L_j$ the length of the bar; $E_j$ the elastic modulus of the bar and $\delta_j$ is the relative displacement of the fore node of bar '$j$' with respect to its back node.

The initial bar areas of the lattice (Figure 1(b)) to simulate a particulate assembly (Figure 1(a)) under an initially applied boundary load is determined through an iterative procedure as follows. The areas of all bars are set to unity and then the initial boundary load is applied to the lattice.

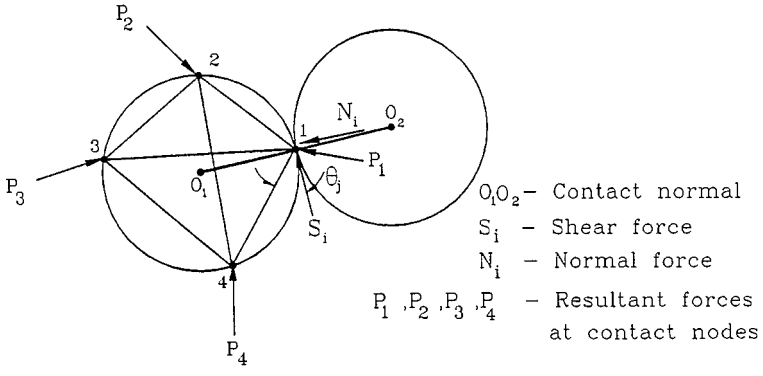


Figure 2. Particle under contact forces

 

A truss analysis is carried out to find the axial forces in the bars. From the axial forces, the contact forces are found as described in the next section. The displacements at the contacts are then found and the area for each bar is calculated from equation (1). An iterative procedure then follows with the boundary load reapplied with the new bar areas. The truss is reanalysed, the bars areas are updated and the process is repeated until the bar areas converge.

The loads in a particulate material flow through contacts between particles pressed together by compressive forces. Thus the load flow between contacts in a particle shown in Figure 2 is through compressive stresses within the particle. In the simulation using the LTM, a bar can develop a very small tensile force when load flow between two contacts is ceased. Under such condition, the axial force in that bar is set to zero and the unbalanced forces are redistributed through an initial load analysis. The area of the bar is then reduced to a low value (a parametric study showed that $10^{-8}$ times the maximum cross-sectional area of the maximum bar area within the lattice was an appropriate reduction factor) so that no load transfer takes place along the direction of this bar. The acronym "weakbar" is used to denote this reduced area.

*Normal force, Shear force and Shear force ratio*

The direction of the resultant force vector from the network within a particle at a contact node represents the load path/contact force on that particle and this is determined by taking the vector sum of the axial forces in the bars. The contact force can be resolved into two components in the direction of contact normal (normal to the contact surface developed when two particles are pressed together with a contact force) and in the direction tangential to the contact normal (shear forces) as shown in Figure 2. The normal and shear forces at a contact are obtained by

$$N_i = \sum_{j=1}^{n-1} F_j \sin \theta_j \tag{2}$$

$$S_i = \sum_{j=1}^{n-1} F_j \cos \theta_j \tag{3}$$

where $N_i$ is the normal force at the contact node '$i$'; $S_i$ is the shear force at the contact node '$i$'; $F_j$ is the axial force in bar '$j$'; $\theta_j$ the angle made by bar '$j$' with the shear force direction at the contact node '$i$'; $n$ the number of contacts around a particle. The shear force ratio ($r_i$) is defined as the absolute value of the ratio of the shear force divided by the normal force. When the shear force ratio exceeds the coefficient of friction ($\mu$) at a contact between two particles, that contact then becomes a sliding one. Since the contact area for the computation of the contact shear and normal stresses are the same, the shear stress ratio is equal to the shear force ratio.

*Nodal constraints*

If the shear stress ratio at a contact node exceeds the coefficient of friction of the material ($\mu$) and a mechanism that would allow relative sliding of particles at contacts has not yet developed, the additional shear force is redistributed to the other contacts by applying an equal and opposite shear force at the contact given by

$$\Delta S_i = (r_i - \mu) N_i \tag{4}$$

 

where $\Delta S_i$ is the additional shear force at the contact node '$i$', $r_i$ is the shear stress ratio and $N_i$ is the normal force. The additional shear force is applied opposite to the shear force at the contact node and resolved into the bars as axial forces relative to the stiffness of the bars. An initial stress analysis is then carried out. An iterative process is required to ensure that the shear stress ratio does not exceed '$\mu$' at any node.

When the normal force at a contact node becomes zero, the contact is deactivated (no load transfer between nodes) and the contact node is split into two nodes; one node for each particle. Constraints are imposed to check for reactivated contacts based on the geometry of the particles. Various algorithms are available for contact detection.[31–33] In the present situation, the particles are assumed to be disks of circular cross section. By keeping track of the location of the centroid of each disk, one can determine whether two particles (disks) reestablish their contacts. The areas of bars linked to the deactivated contacts are set equal to 'weakbar'.

*Kinematics*

The lattice-type simulation of the particulate assembly described so far cannot simulate the kinematics (sliding, rotation and rolling) of the particles. There must be nodal offsets at the joints to account for the kinematics. One can appeal to or adopt kinematic techniques used in robotics, for example Tanaka *et al.*[34] However, in this paper, we have taken a simplified and novel approach by reconfiguring the truss (Fig. 1(b)) into a framework that represents a mechanism capable of simulating the kinematics. The resultant of the rigid-body motion and the elastic deformation of the particles drives the motion of the mechanism.

A mechanism for the kinematics is developed when an increment of shear displacement produces no increase in shear force or vice versa, or when an increment of axial strain produces no increase in axial stress. When this occurs, further deformation is traced kinematically through a mechanism framework formed by introducing nodes at particle centroids and linking them with bars. The stiffnesses of bars linking particle centroids with active non-sliding contacts are made very large or 'infinite' (we found that using a relative stiffness value of $10^8$ was effective) relative to the stiffness of bars (unity) linking particle controids with sliding contacts. During the deformation of the mechanism framework, relative displacements occur between particle centroids as well as at particle contacts and thus this framework simulates the relative sliding, rotation, and rolling of particles in a global approach. Mechanism frameworks at various stages of deformation for particulate assemblies discussed later in this paper are presented in Ramakrishnan.[26]

In order to explain the concept of the mechanism framework further, consider an assembly of disks representing quartz grains under simple shear (Figure 3(a)). If a mechanism develops in this assembly, say when all the vertical planes become sliding planes, then the kinematics of this deformation is simulated by the mechanism framework shown in Figure 3(b). Bars-linking particles with sliding contacts have stiffnesses of unity while bars linking particles with non-sliding contacts have large stiffnesses (of $10^8$). The framework is then subjected to a small displacement (simple shear) under the appropriate boundary conditions and then analysed. The co-ordinates of the centroids of the particles are then updated from the new centroidal coordinates. The axial forces in the bars, prior to the development of the mechanism, are used as initial bar forces and an initial load analysis is carried out to reestablish equilibrium in the reformulated lattice. The new shear stress ratios at the contacts are then computed and incremental load is applied. The approach taken to handle kinematics in this paper is a simplified approach and has

 

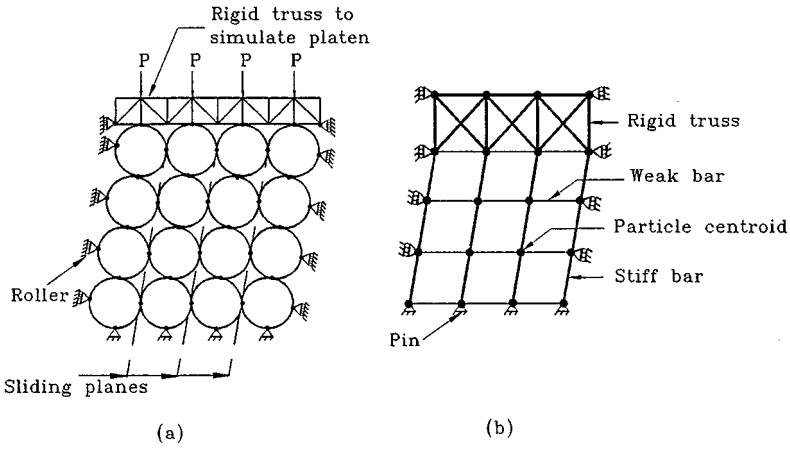


Figure 3. (a) Loose packing under simple shear; (b) Mechanism framework

given satisfactory results for the problems considered in this paper. The authors are now considering a more elaborate approach to handle particle kinematics through structural frameworks using ideas derived from robotics.

*Numerical procedures*

The major numerical procedures and their links in the lattice-type model are shown in the flow chart in Figure 4. The displacements of the nodes in the truss analysis was solved using the Gaussian elimination method. In the LTM, the stiffness matrix has to be reformed at the end of each analysis due to the updating of bar areas and contact deletions or additions. In this context, it is to be mentioned that Vinogradov and Gavrilov[35] developed a method in which the stiffness matrix was updated after each contact delection or addition rather than recalculation of the new stiffness matrix which led to computational efficiency.

*Application to two-dimensional arrays of particles*

The lattice-type model is applied here to two-dimensional assemblies of circular disks of radius 2·54 mm (0·1 in). The disks are arranged into the loosest packing consisting of 96 particles and the densest packing consisting of 104 particles (Figure 5). Quartz is assumed to be the material with the following properties;[36] elastic modulus ($E$) = 46·0 GPa; Poisson's ratio ($v$) = 0·20; shear modulus (G) = 19·2 GPa; friction coefficient ($\mu$) = 0·50. The assemblies of disks were replaced by a truss as shown for the dense assembly in Figure 6. For each assembly, a constant vertical load was imposed followed by increments of a triangular distribution of displacements at the lateral boundaries (Figure 6) to simulate simple shear loading conditions. A rigid truss at the top boundary was used to simulate the top load platen. The particle contacts at the bottom boundary

 

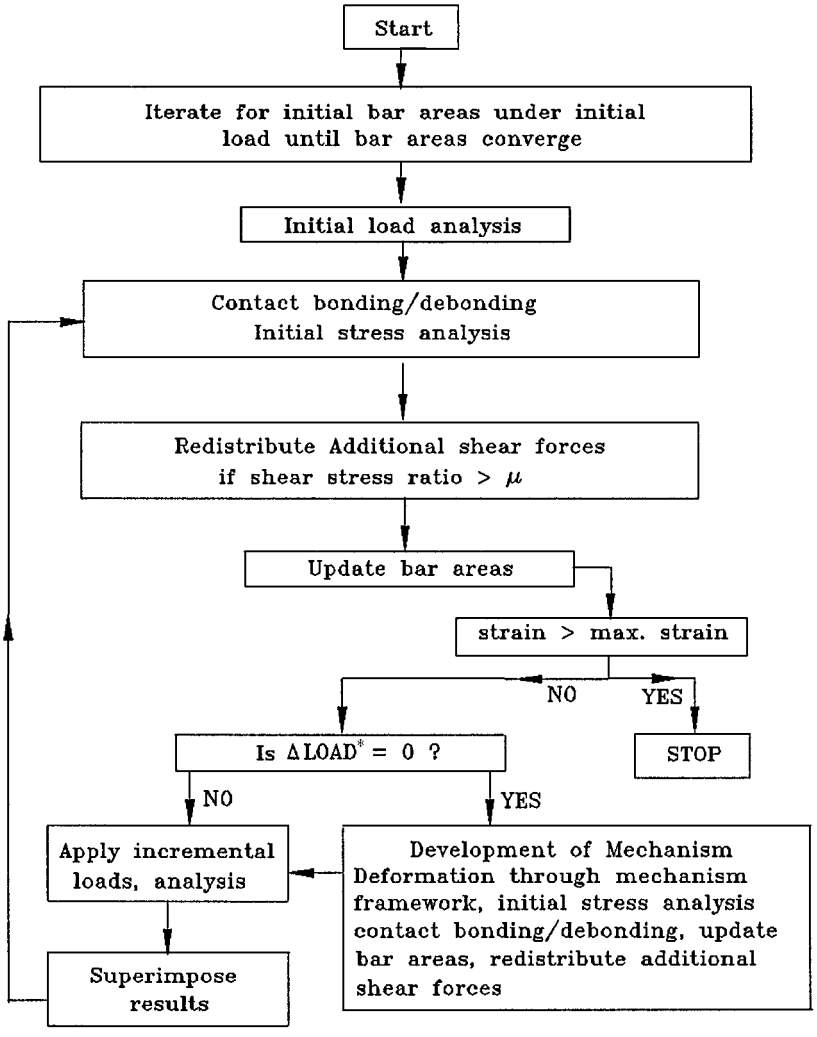


Figure 4. Flow chart of numerical procedures in the lattice-type model (*ΔLOAD = change in load)

were simulated by hinges. The assemblies were given freedom to move only in the vertical direction by simulating the lateral boundaries as rollers.

The above assemblies were also analysed using a commercially available program (PFC-2D from Itasca Consulting Group) based on DEM in which deformation of a particulate assembly is simulated using a dynamic approach. Simple shear was simulated by setting an angular velocity for the vertical boundaries and a linear velocity for the top platen. The following data set for the linear model option were used: density = 2000 kg/m$^3$; angular velocity = $5 \times 10^{-8}$/s; $\mu = 0{\cdot}5$; normal stiffness = $1{\cdot}5 \times 10^8$ N/m; shear stiffness = $1{\cdot}2 \times 10^8$ N/m.

 

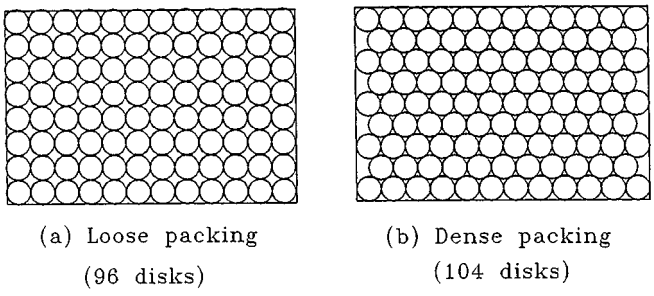


Figure 5. Loose and dense packings

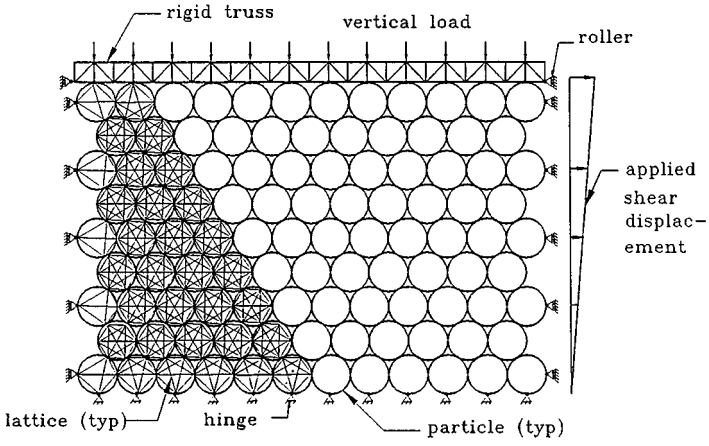


Figure 6. Simulation of simple shear

*Load paths*

The resultant force vector at each contact constitutes the 'load path' through a particle. The results of the load paths for the dense packing from LTM and DEM are shown in Figures 7–11 under the vertical load and at shear strains ($\gamma$) of 0·01, 0·04, 1 and 5 per cent, respectively. The thickness of lines in these diagrams indicates the magnitude of the contact forces relative to the maximum contact force in the disk assembly. The scales used for the line thicknesses in the two models are very close. The scales used in the PFC-2D program is fixed in the program and this is unknown to the authors, so an exact common scale could not be used. The disks are superimposed on the load paths to show how the packing structure (fabric) evolved up to the level of shear strains indicated. The load paths show that the loads are supported by columns of particles and some clusters of particles do not carry any load (clusters at the bottom right and top left corners). This agrees with observations in simple shear tests on sands[37] in which it was observed that regions near the corners of the longer diagonal are stress free. The distribution of contact forces at the boundaries (Figures 8–11) under simple shear shows that the contact forces increase from zero

 

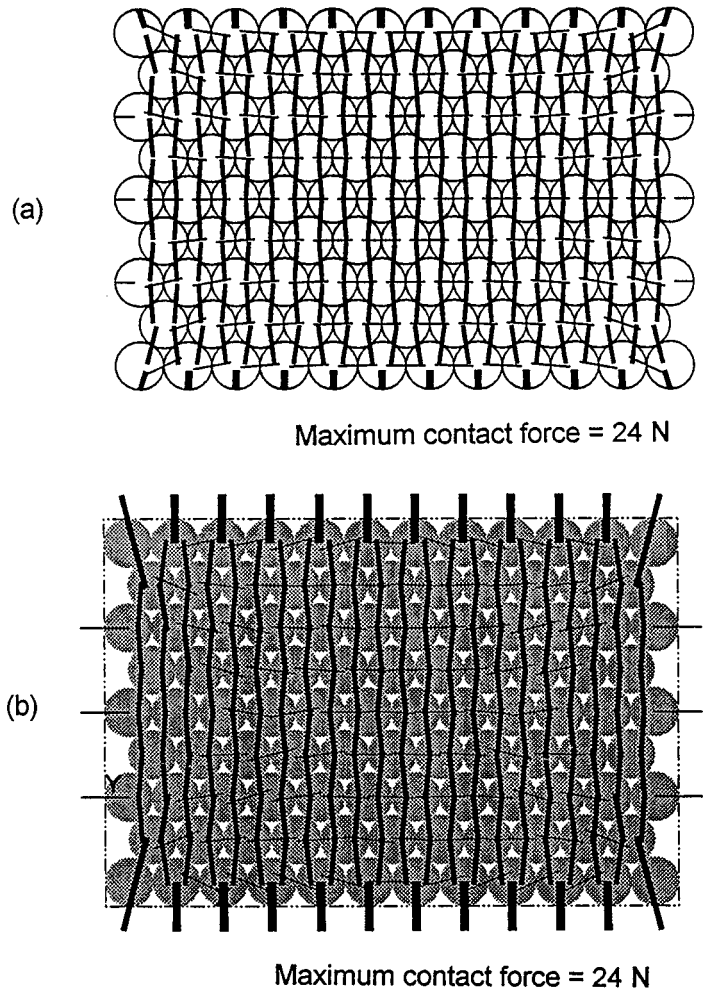


Figure 7. Load paths for dense packing under vertical load from: (a) LTM; (b) DEM

at left bottom to a maximum at the right bottom and *vice versa* at the top boundaries. The non-uniform distribution of contact forces at boundaries predicted by the LTM are compatible with the results of simple shear tests on sands.[37]

Two distinct sets of load paths appear under simple shear. One set of paths is approximately parallel to a line AA while the other set of paths is approximately parallel to a line BB (Figure 8(a)). The contact forces at contacts along paths parallel to BB tend to decrease while the contact forces at contacts parallel to AA tend to increase. At $\gamma \geqslant 0{\cdot}04$ per cent contacts along paths parallel to BB become deactivated and the loads are only transmitted along a band of contacts parallel to AA (Figures 9 and 10). At a shear strain of 5 per cent (Figure 11), void spaces appear between some contacts along lines parallel to BB. The results from the LTM match the results from DEM very closely for shear strains less than 1 per cent. The DEM results show a sudden

 

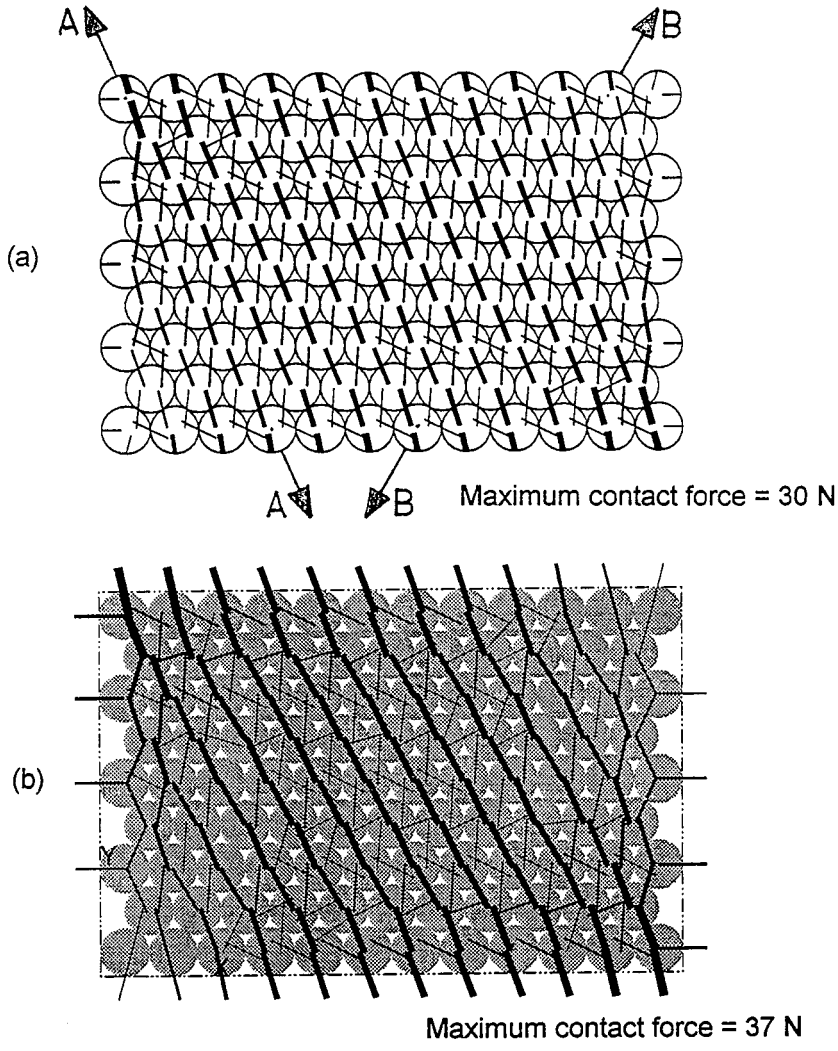


Figure 8. Load paths for dense packing at $\gamma = 0{\cdot}01$ per cent from; (a) LTM; (b) DEM

degeneration of the load paths from an established pattern (inclined columns of disks that rotate about the bottom boundary) just before $\gamma = 1$ per cent. In the DEM, a particle movement is calculated from the acceleration resulting from the resultant force and moment in the particle.[13] Kishino[13] stated that the particle motion is 'not co-axial with the acceleration vector because of the constraints by neighbouring grains and/or boundary $\cdots$ and may affect results for dense assemblies of grains.' This perhaps is the reason for the sudden change in load paths obtained from DEM. Photoelastic experiments, using a simple shear device, were conducted on a dense packing of 53 photoelastic disks.[38] The fringe patterns show load paths similar to those predicted

 

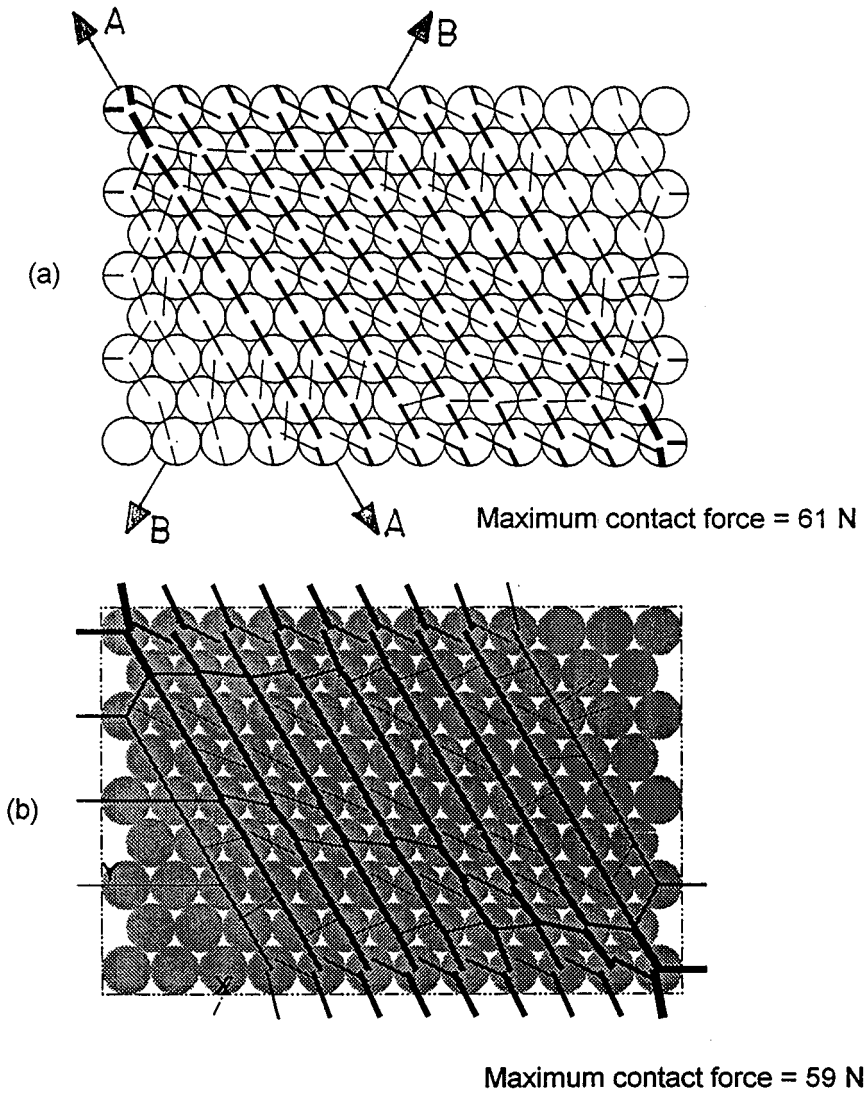


Figure 9. Load paths for dense packing at $\gamma = 0{\cdot}04$ per cent from (a) LTM; (b) DEM

by LTM. At large shear strains (Figure 12), we did not observe any degeneration of the load paths from the established pattern of chains of disks rotating about the bottom boundary.

Load paths for the loose packing under a vertical load are shown in Figure 13 and in Figures 14 and 15 at shear strains ($\gamma$) of 1 and 50 per cent. The major load paths, when the vertical load is applied, are vertical (Figure 13), as expected, and both models show good agreement. At $\gamma = 1$ per cent (Figure 14(a)), the LTM results show that particle sliding occurs on planes that were initially

 

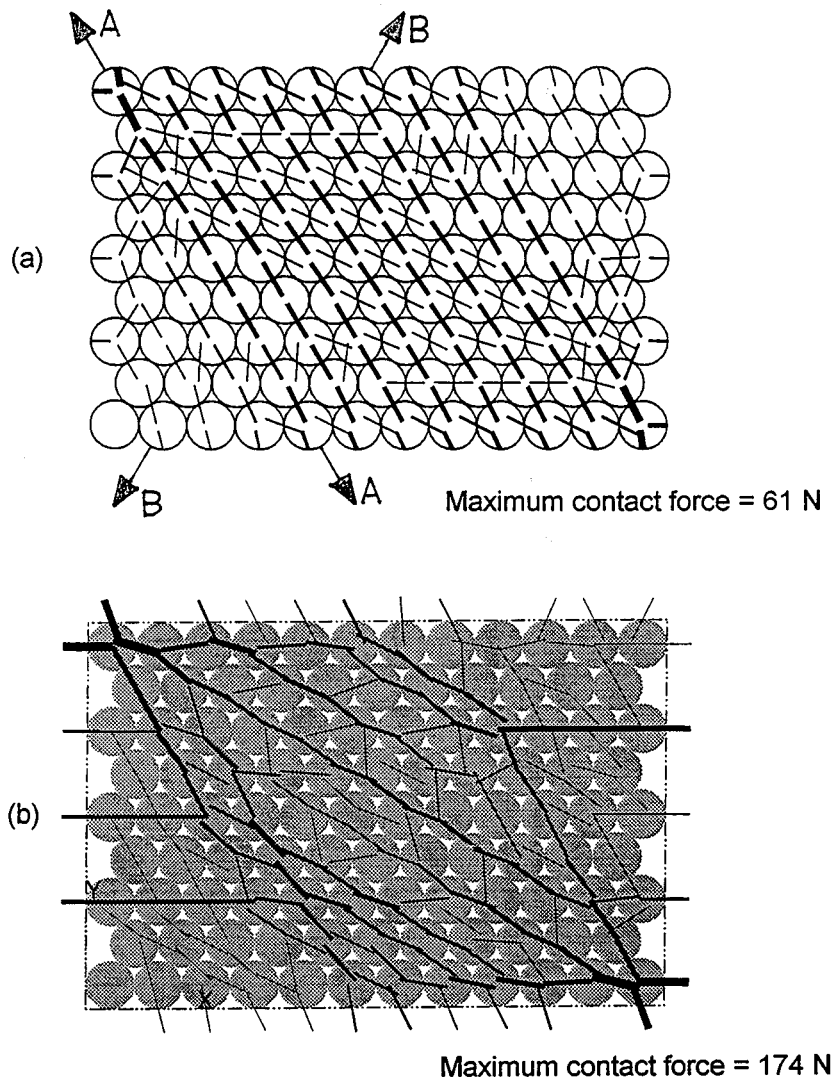


Figure 10. Load paths for dense packing at $\gamma = 1$ per cent from; (a) LTM; (b) DEM

vertical and the particles rotate about the bottom boundary as adjoining columns. Each column of disks slips into the voids space made available by the forward (in the direction of shear) column. The load paths predicted by DEM are irregular (Figure 14(b)) with significant loads transferred in the lateral direction. As the shear strain is increased, the load paths from LTM resemble a staircase with sloping runners and at $\gamma = 50$ per cent (Figure 15) the loose assembly reaches its closest packing. At this stage, the lateral forces in most disks are equal to the vertical forces suggesting a hydrostatic condition.

 

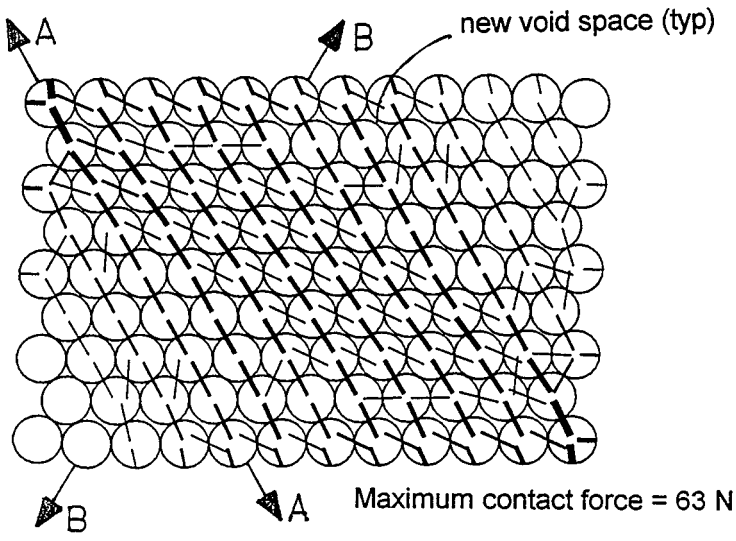


Figure 11. Load paths for dense packing at $\gamma = 5$ per cent from LTM

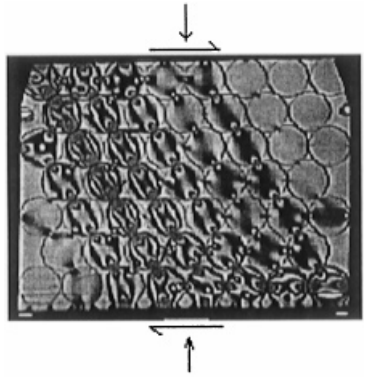

Figure 12. Fringe patterns at $\gamma = 3$ per cent from photoelastic experiments in a simple shear device

*Stress–strain and volume change response*

The results of numerical tests using the lattice-type model yield a discrete set of forces and their locations. Hill's averaging principle, as applied by Drescher and de Jong,[39] can be used to transform the discrete set of contact forces to an equivalent state of stress in a two-dimensional continuum element.[26] However, in this paper, we present results of the average shear stress ratio (total shear force/total normal force) at the bottom boundary as this is representative of the shear stress ratio that would be determined from measurements made with load cells placed at the

 

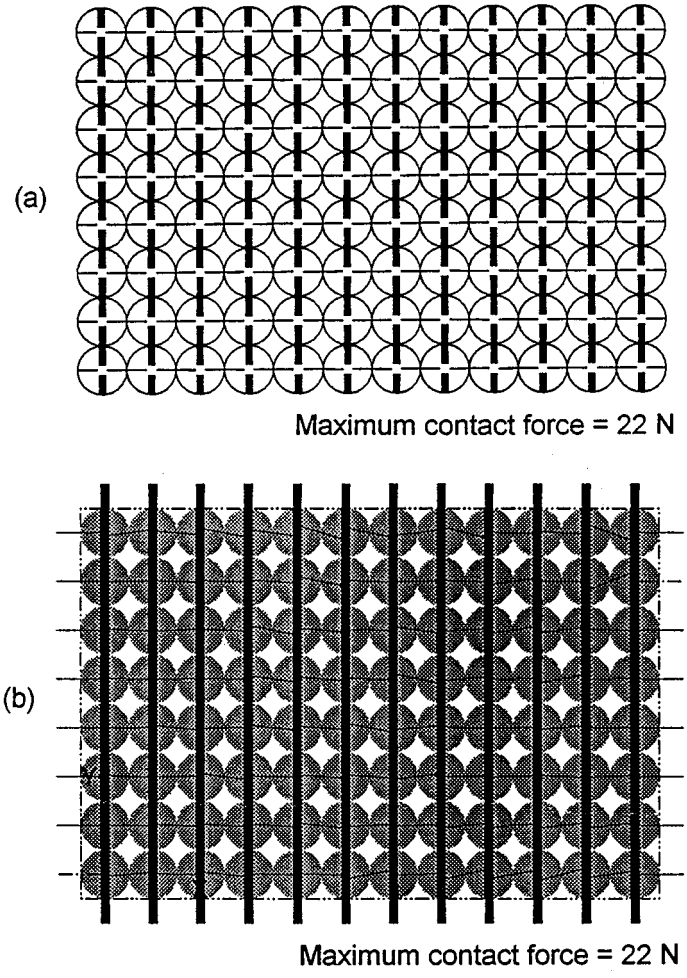


Figure 13. Load paths for loose packing under vertical load from; (a) LTM; (b) DEM

bottom boundary of simple shear testing devices.[37] The variations of the shear stress ratio and the volumetric strain obtained from LTM and DEM for the dense packing are shown in Figure 16 and they match closely. The volumetric strain, $\varepsilon_v$, was computed from the vertical movement, $\delta y$, of the top platen (top rigid truss) as

$$\varepsilon_v = \frac{\delta y}{h} \tag{5}$$

where $h$ is the height of the assembly. Since the packing is the densest one possible, the disk assembly shows no compression and dilates once shear displacements were applied. The tangent

 

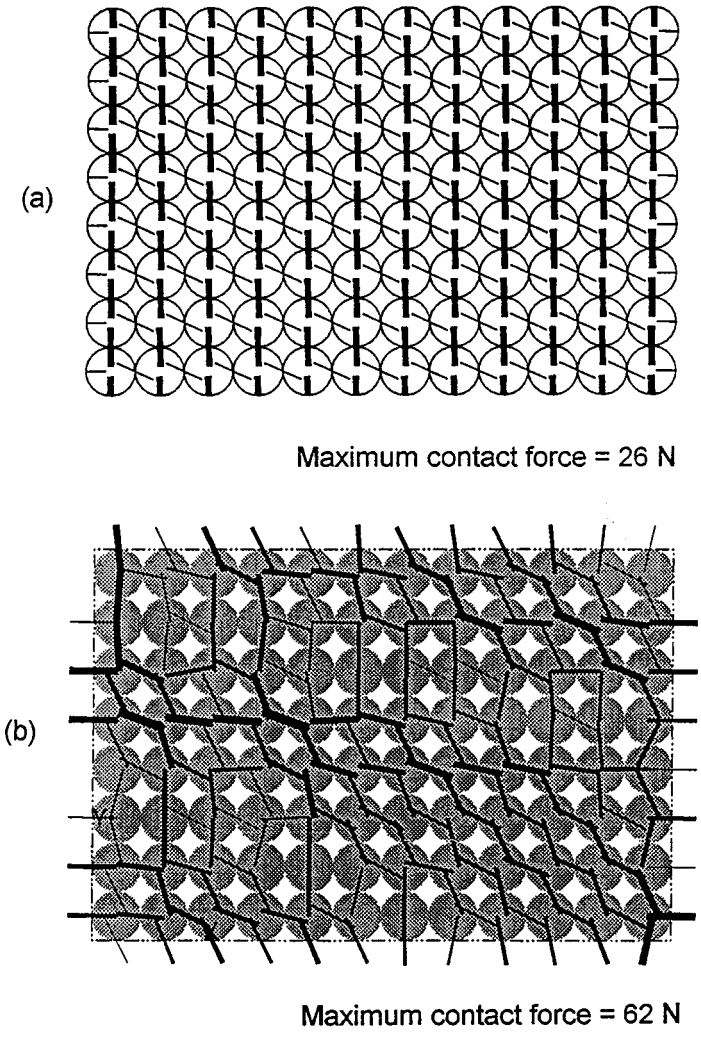


Figure 14. Load paths for loose packing at $\gamma = 1$ per cent from; (a) LTM; (b) DEM

shear modulus is 287 MPa from the initial part of the stress–strain curve (Figure 16) and is within the range of typical values for sandstones.[40]

*Constraint ratio*

Cundall and Strack[8] proposed the term called 'constraint ratio' to check the development of a mechanism in a granular assembly as

$$\mathrm{CR} = \frac{C(2 - S)}{3N} \tag{6}$$

 

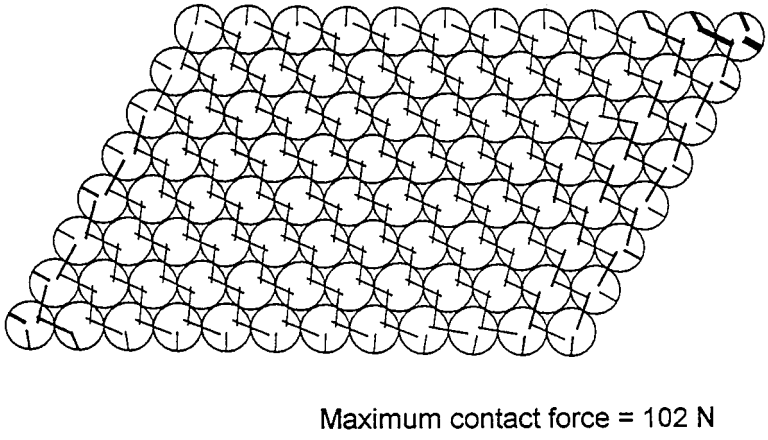


Figure 15. Load paths for loose packing at $\gamma = 50$ per cent from LTM

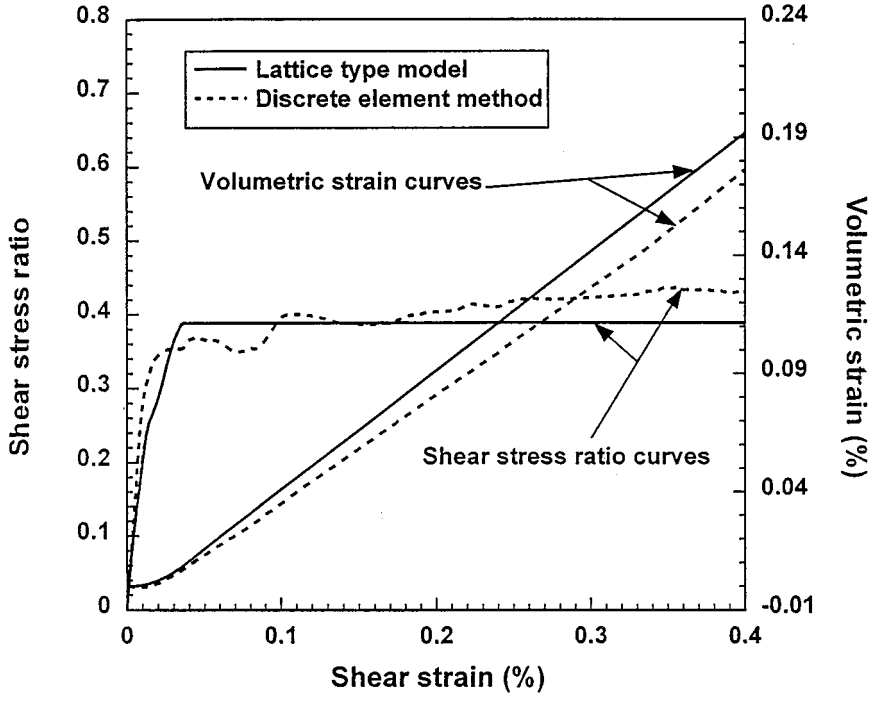


Figure 16. Variation of shear stress ratio and volumetric strain for dense packing

where $N$ is the number of particles, $C$ is the number of contacts, $S$ is the fraction of sliding contacts to the total number of contacts. In the numerical tests using DEM, Cundall and Strack[8] showed that CR = 1 when a mechanism develops in a granular assembly. The values of CR calculated from the LTM results up to $\gamma = 0{\cdot}1$ per cent are shown in Figure 17. The constraint ratio begins

 

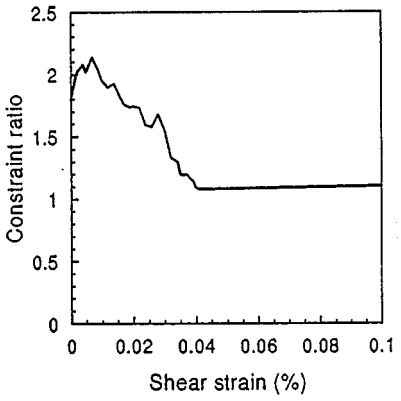


Figure 17. Variation of constraint ratio for dense packing

with a value of 1·8 at $\gamma = 0$, zigzags up to a maximum value of 2·2 at $\gamma = 0{\cdot}007$ per cent and then decreases to a constant value of 1 at $\gamma \geqslant 0{\cdot}04$ per cent. It was observed from the LTM results that the latter occurs when a considerable number of contacts along lines parallel to BB (Figure 9) becomes deactivated. These LTM results provide an independent verification of the development of a mechanism using the constraint ratio proposed by Cundall and Strack[8] and the suitability of the framework analogy used here to describe the kinematics in LTM.

*Study of initial imperfections*

In nature, finding homogenous materials is rare and most granular geomaterials are composed of particles with different sizes, shapes and stiffnesses. In the discrete element method, when two particles of different elastic moduli are in contact, the contact stiffnesses are computed by taking an average elastic modulus since the contacts are modeled rather than the particles. In the LTM, a lattice simulates each particle and thus there is no need for an averaging procedure for the elastic moduli of the particles.

To demonstrate the applicability of LTM to study the effects of particles with different elastic modulus termed 'initial imperfections' here, two cases of the dense packing in Figure 5(b) are considered. In the first case, the elastic modulus of 4% of the particles, selected orderly (Figure 18), was set to a value of 0·46 GPa (1/100th of the elastic modulus of other particles) and in the second case, the elastic modulus of 25 per cent of the particles, randomly selected, are set equal to 0·46 GPa. We will call these particles 'weak particles' and the particles assemblies with initial imperfections as heterogeneous assemblies.

The load paths from the LTM under a vertical load and at a shear strain of 1% for the heterogeneous assemblies are shown in Figures 18 and 19. These figures should be compared with Figure 7(a) and 10(a), respectively for the homogeneous packing. The major load paths for the heterogeneous packing with 25 per cent imperfections (Figure 19) are weaved through a network of contacts along the stronger particles avoiding the weaker particles. Each load path carries larger loads in the heterogeneous assembly as compared with the homogeneous assembly because the percentage of particles participating in actively transferring the load is reduced in the

 

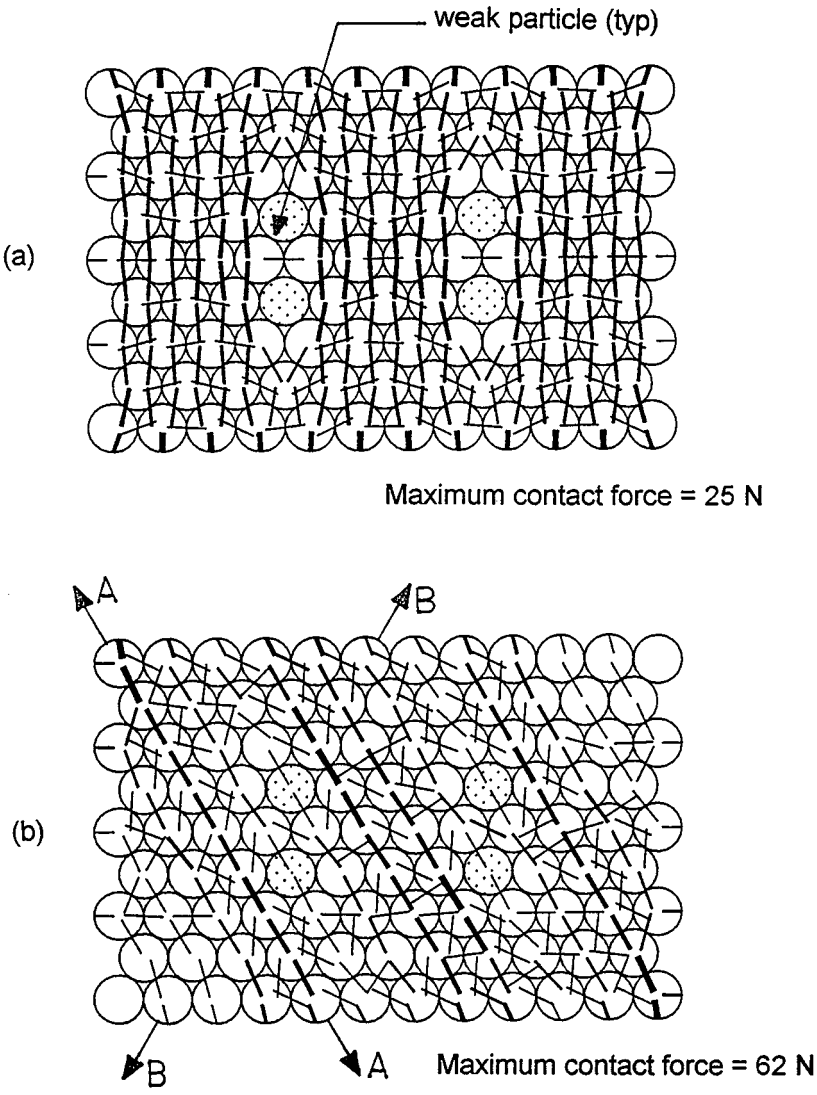


Figure 18. Load paths for dense packing with 4 per cent initial imperfections under; (a) vertical load; (b) $Y = 1$ per cent

heterogeneous assembly. For example, the maximum contact force in the homogeneous assembly is 24N compared with 54N for the heterogeneous assembly (Figure 19(a)) under vertical loads only. In the packing with 4 per cent imperfections at a shear strain of 1 per cent (Figure 18(b), load flows predominantly through four major load paths along line AA. The load paths through the weak particles are sandwiched between the four major load paths and their role appears only to provide lateral stability to the major load paths during deformation.

 

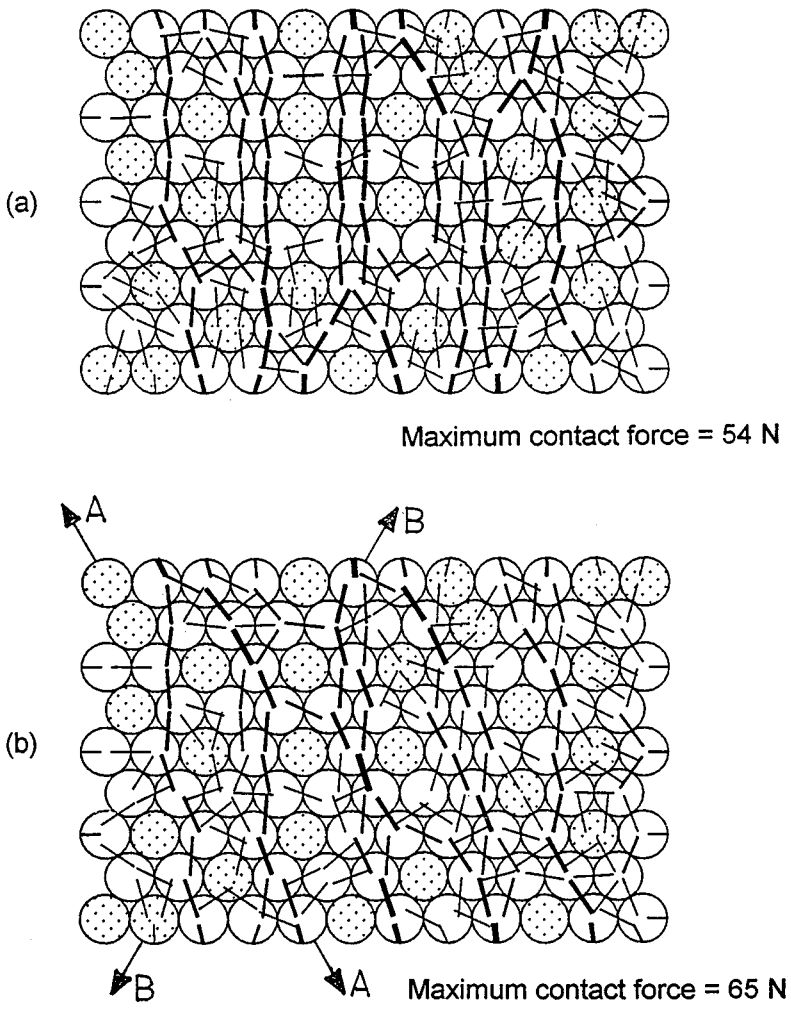


Figure 19. Load paths for dense packing with 25 per cent initial imperfections under; (a) vertical load; (b) $Y = 1$ per cent

The stress–strain behaviour for the homogeneous and the two heterogeneous assemblies are shown in Figure 20 in which the average shear stress ratio at the bottom plane is plotted. The shear modulus for the 4 per cent heterogeneous packing and the homogeneous packing is the same and thus a 4 per cent imperfection does not seem to have any negative affect on the initial material response. However, the maximum shear stress ratio is reduced by the imperfections because a mechanism develops earlier from the reduction in the number of major load paths (Figure 18(b)) compared with the homogeneous packing. For the packing with 25 per cent imperfections, the shear modulus and the maximum shear stress ratio are reduced. The shear modulus for this assembly is 94 MPa compared to 287 MPa for the homogeneous assembly. These reductions are attributed to the reduction in the number of active contacts in the direction

 

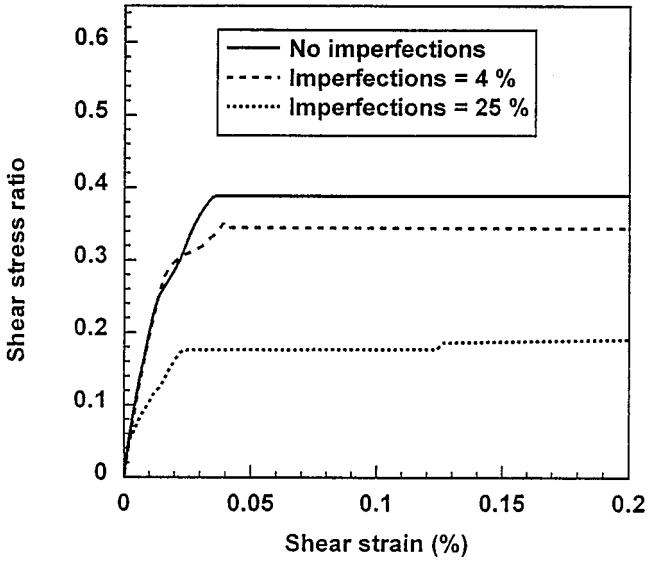


Figure 20. Stress–strain behaviour for dense packings with initial imperfections

of shorter diagonal (line BB) in the heterogeneous packing compared with the homogeneous packing.

## CONCLUSIONS

A lattice-type model to study the micro-mechanical behaviour of particulate media has been developed and numerical tests have been conducted on dense and loose assemblies of disks. In the LTM, a particulate assembly is transformed into a truss and is analyzed using standard methods in structural mechanics along with the imposition of certain nodal constraints and a novel mechanism framework approach for the kinematics of particles. The important features of the model are (1) a conceptually simple model that uses established methods of analysis in structural mechanics (2) the particulate medium itself is simulated (represented by a network of bars of representative stiffness) unlike other existing methods, such as the Discrete Element Method, where the particles are replaced by springs at the contacts. This feature in LTM is especially important if one wishes to consider phenomena such as particle (or grain) crusing and initial particle imperfections.

An example showing how LTM can be used to study initial imperfections reveal that with only 25 per cent of particles with elastic modulus two orders of magnitude lower produce 67 per cent lower shear modulus than a homogeneous packing. A future application of the LTM could be to the study of particle crushing which can be carried out by redistribution of the contact forces from the crushed particle and reducing the bar areas of the same to 'weakbar'. The results of numerical tests from LTM concord well with the results using the DEM for the dense packing at low shear strains and with the results of photoelastic experiments.

The LTM has not been tested at deformations at which the particles can break many contacts and create new ones, and it is not known how well the model will perform under this

 

circumstance. Further studies are underway to test the model performance and robustness for a wide range of problems, including particle crushing and structural arrangements.

ACKNOWLEDGEMENTS

This work was sponsored by the Air Force Office of Scientific Research and by the National Science Foundation. The authors are grateful to program managers, Lt. Col. Martin Lewis (AFOSR) and Dr. Mehmet T. Tumay (NSF), at the time awards were made, for their support of this research.

## APPENDIX I

*Displacements in an elastic disk*

Michell[29] derived expressions for stresses in a disk acted upon by a contact force '*P*' (Figure 21) which is held in equilibrium by a radial compressive stress with a distribution of magnitude $(2P/\pi f)\cos\theta_1)/r_1$ in which '*t*' is the thickness of the disk and $\theta_1$ and $r_1$ are as shown in Figure 21. The rectangular components of the stresses $\sigma_x$, $\sigma_y$ and $\tau_{xy}$ at any point $(x, y)$ in the disk are given by

$$\sigma_x = -\frac{2P}{\pi t}\frac{\cos\theta_1}{r_1}\sin^2\theta_1 \tag{7}$$

$$\sigma_y = -\frac{2P}{\pi t}\frac{\cos\theta_1}{r_1}\cos^2\theta_1 \tag{8}$$

$$\tau_{xy} = -\frac{2P}{\pi t}\frac{\cos\theta_1}{r_1}\sin\theta_1\cos\theta_1 \tag{9}$$

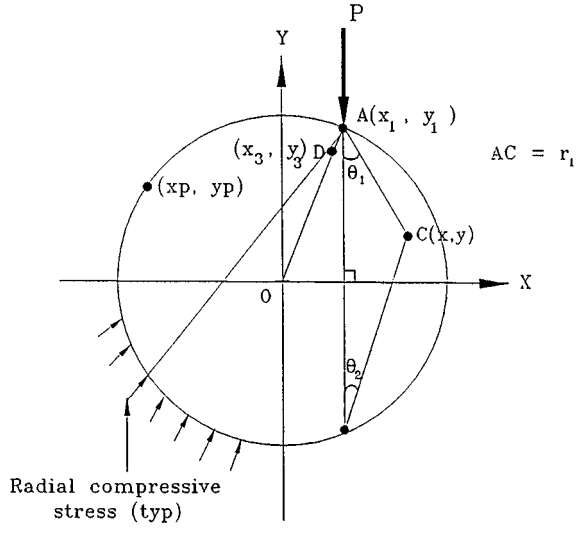


Figure 21. Elastic disk under a contact force

 

where $r_1^2 = (x - x_1)^2 + (y - y_1)^2$. The stresses in a disk acted upon by a system of contact forces on its boundary (Figure 2) can be obtained by the superposition of the stresses given by the above equations under each load $P_i$ and adding to them an isotropic tension given by $\sum_{i=1}^{n} (P_i/\pi td) \sin(\theta_1 + \theta_2)$[29] in which '$d$' is the diameter of the disk, '$n$' is the number of contact nodes and $\theta_1$, $\theta_2$ are as shown in Figure 21. The displacement gradients are then given by

$$\frac{\partial u}{\partial x} = \varepsilon_x = \frac{1}{E}(\sigma_x - v\sigma_y) \tag{10}$$

$$\frac{\partial v}{\partial y} = \varepsilon_y = \frac{1}{E}(\sigma_y - v\sigma_x) \tag{11}$$

where $u$ and $v$ are the $x$ and $y$ components of the displacements; $\varepsilon_x$, $\varepsilon_y$ are the strains in the $x$ and $y$ directions; $E$ and $v$ are the elastic modulus and Poisson's ratio of the material of the disk. The displacements, $u$ and $v$, at a general point ($xp$, $yp$) are obtained by integrating the displacement gradients between this point and a point where $u$ and $v$ displacements are zero. However, due to rigid-body motion of the disk, it is not possible to determine the absolute value of the displacement of any point on the disk. Therefore, only relative displacements of points ($xp$, $yp$) with respect to the centroid of the disk are determined. The displacements, $u$ and $v$, are then

$$u = \int_0^{xp} \frac{\partial u}{\partial x}\,\mathrm{d}x \tag{12}$$

$$v = \int_0^{yp} \frac{\partial v}{\partial y}\,\mathrm{d}y \tag{13}$$

The displacement of point, A, with respect to the centroid O is obtained by integrating the above expressions from (0, 0) to ($x_1$, $y_1$). However, this will lead to singularity and thus, theoretically, it is not possible to determine the displacement of A relative to the centroid O. The stresses are also singular at point A. Therefore, the displacement at A is evaluated as a sum of the displacement at the yield point ($x_3$, $y_3$) and the product of the displacement gradient at D and the projected length of DA in the $x$ and $y$ directions. The displacements of A are given by

$$u_A = u_D + \left.\frac{\partial u}{\partial x}\right|_{(x_3, y_3)} (x_1 - x_3) \tag{14}$$

$$v_A = v_D + \left.\frac{\partial v}{\partial y}\right|_{(x_3, y_3)} (y_1 - y_3) \tag{15}$$

where $u_A$, $v_A$ and $u_D$, $v_D$ are the $x$ and $y$ components of the displacements at A and D, respectively. The yield point ($x_3$, $y_3$) is determined by setting the expression for major principal stress along the line OA equal to the yield stress of the material of the disk.

## REFERENCES

1. G. Frantziskonis, P. Karpur, T. E. Matikas, S. Krishnamurthy and P. D. Jero, 'Fiber-matrix interface – information from experiments via simulation', *Compos. Struct.*, **29,** 231–247 (1994).
2. K. L. Johnson, *Contact Mechanics*, Cambridge University Press, Cambridge, 1985.

 

3. A. A. Serrano and J. M. Rodriguez-Ortiz, 'A contribution to the mechanics of heterogeneous granular media', *Proc. Symp. on Plasticity and Soil Mechanics*, Cambridge, UK (1973).
4. R. D. Mindlin, 'Compliance of elastic bodies in contact', *J. Appl. Mech*., 259–268, (1949).
5. P. A. Cundall and O. D. L. Strack, 'A discrete numerical model for granular assemblies', *Geotechnique*, **29,** 47–65, (1979a).
6. P. A. Cundall and O. D. L. Strack, 'The development of constitutive laws for soils using the distinct element method', in Aachen (ed), *Numerical Methods in Geomechanics*, W. Wittke, 1979b, pp. 289–298.
7. P. A. Cundall, A. Drescher and O. D. L. Strack, 'Numerical experiments on granular assemblies; Measurements and observations', in P. A. Vermeer and H. J. Luger (eds.), *Proc. IUTAM Conf. on Deformation and Failure of Granular Materials*, Delft, A. A. Balkema, Rotterdam, 1982, pp. 355–370.
8. P. A. Cundall and O. D. L. Strack, 'Modelling of microscopic mechanisms in granular material', in J. T. Jenkins and M. Satake (eds), *Mechanics of Granular Materials*, Elsevier, Amsterdam, 1983, pp. 137–149.
9. C. Thornton and D. J. Barnes 'Computer simulated deformation of compact granular assemblies', *ACTA Mech*., **64,** 45–61 (1986).
10. J. P. Bardet and J. Proubet, 'An adaptative relaxation technique for the statics of granular materials', *Comput. Struct*., **39** (3/4), 221–229 (1991).
11. R. J. Bathurst and L. Rothenburg, 'Micro-mechanical aspects of isotropic granular assemblies with linear contact interactions', *J. Appl. Mech*., **55,** 17–23 (1988).
12. C. S. Chang and A. Mishra, 'Computer simulation and modelling of mechanical properties of particulates', *Comput. Geotech*., **4,** 269–287 (1989).
13. Y. Kishino, Disc model analysis of granular media', in M. Satake and J. T. Jenkins (eds), *Micromechanics of Granular Materials*, Elsevier, Amsterdam, 1988, pp. 143–152.
14. M. D. Adley and M. H. Sadd, 'Continuum models for materials with lattice-like microstructure', *Comput. Struct*., **43** (1)**,** 13–18 (1992).
15. H. Dai and G. Frantziskonis, 'Heterogeneity, spatial correlations, size effects and dissipated energy in brittle materials', *Mechanics of Materials*, Elsevier, Amsterdam, 1994, pp. 103–118.
16. H. J. Herrmann and S. Roux, '*Statistical Models for the Fracture of Disordered Media*, North-Holland, Amsterdam, (1990).
17. D. Krajcinovic and M. A. Silva, 'Statistical aspects of the continuous damage theory', *Int. J. Solids Struct*., **18** (7), 551–562 (1982).
18. D. Krajcinovic and M. Basista, 'Rupture of central-force lattices revisited', *J. Phys. I*, **1,** 241–245 (1991).
19. M. H. Sadd, L. Qui, W. G. Boardman and A. Shukla, 'Modelling wave propagation in granular media using elastic networks', *Int. J. Rock. Mech. Min. Sci. Geomech. Abstr*. **29** (2), 161–170 (1992).
20. D. H. Trollope and B. C. Burman, 'Physical and numerical experiments with granular wedges', *Geotechnique*, **30,** 137–157 (1980).
21. A. Hrennikoff, 'Solution of problems of elasticity by the framework method', *J. Appl. Mech. ASME*, A-169–175 (1941).
22. N. M. Newmark, 'Numerical methods of analysis in bars, plates and elastic bodies', in L. E. Grinter (ed), *Engineering* Macmillan, New York, 1949.
23. L. Kollar and I. Hegedus, *Analysis and Design of Space Frames by the Continuum Method*, Elsevier, Amsterdam, (1985).
24. J. O. Dow, Z. W. Su, C. C. Feng and C. Bodley, 'Equivalent continuum representation of structures composed of repeated elements', *AIAA J*., **23,** 1564–1569 (1985).
25. A. K. Noor and W. C. Russell, 'Anisotropic continuum models for beamlike lattice trusses', *Comput. Methods Appl. Mech. Engng*., **57,** 257–277 (1986).
26. S. Ramakrishnan, 'Mechanics of particulate media—A lattice type approach', *Ph.D. Thesis*, Department of Civil Engineering and Engineering Mechanics, University of Arizona, Tucson, AZ, (1977).
27. M. Budhu, S. Ramakrishnan and G. Frantziskonis, 'Mechanics of particulate media – a lattice type approach', *Proc. Workshop on Mechanics and Statistical Physics of Particulate Materials*, Institute for Mechanics and Materials, 1994, pp. 33–36.
28. D. W. Luekens, *Theory and Application of Morphological Analysis*, CRC Press, Boca Raton, FL, (1991).
29. J. H. Michell, *Proc. London Math. Soc*. **32,** 44 (1900).
30. S. P. Timoshenko, and J. N. Goodier, *Theory of Elasticity*, McGraw Hill, New York, 1970, pp. 122–126.
31. J. Bonet and J. Peraire, 'An Alernating Digital Tree (ADT) algorithm for 3D geometric searching and intersection problems', *Int. J. Numer. Methods Engng*., **31,** 1–17 (1991).
32. A. Munjiza, N. Bicanic and D. R. J. Owen, 'BSD contact detection algorithm for discrete elements in 2D', in Williams and Mustoe (eds), *Proc. 2nd Int. Conf. on DEM*, IESL Publications, Boston, 1993, pp. 39–52.
33. L. M. Taylor and D. S. Preece, 'Simulation of blasting induceed rock motion using spherical element models', in Williams/Mustoe (eds), *Proc. 1st US Conf. on DEM*, CSM Press, Goden, Colorado, 1989.
34. M. Tanaka, Y. Seguchi and K. Hanahara, 'Kinematics of adaptive truss permitting nodal offset (configuration and workspace reach)', *J. Intelli Mater* Systems Struct **2** (3), 301–327 (1991).

 

35. O. Vinogradov and D. Gavrilov, 'A cluster in granular systems as a topologically variable structure', *Proc. McNU'97, The 1997 Joint Summer Meeting of the ASME, ASCE, and SES*, Northwestern university U.S.A, 1997.
36. C. L. Mantell, *Engineering Materials Handbook*, McGraw Hill, New York, 1958.
37. M. Budhu, 'Simple shear deformation of sands', *Ph.D. Thesis*, Cambridge University, Cambridge, United Kingdom, (1979).
38. B. Dragoo, 'Two-dimensional photoelastic modelling of granular media using image processing', *M.S. Thesis*, Department of Civil Engineering and Engineering Mechanics, University of Arizona, Tucson, AZ, 1995.
39. A. Drescher and G. De Josselin De Jong, 'Photoelastic verification of a mechanical model for the flow of a granular material', *J. Mech. Phys. Solids*, **20,** 337–351 (1972).
40. L. Dobereiner and M. H. De Freitas, 'Geotechnical properties of weak sandstones', *Geotechnique*, **36** (1), 79–94.
41. N. Bicanic, A. Munjiza, D. R. J. Owen and N. Petrinic, 'From continua to discontinua – A combined finite element/discrete element modelling in civil engineering', *Dev. Comput. Tech. Struct. Engng*., 1–13 (1995).
42. J. Feda, '*Mechanics of Particulate Materials*', Elsevier, Amsterdam, 1982.

 